Electrochemical and Solid-State Letters, **13** (3) C1-C3 (2010)
1099-0062/2009/13(3)/C1/3/$28.00 © The Electrochemical Society

Intergranular Corrosion Resistance of Σ3 Grain Boundaries in Alloy 22

P. Jakupi,[z] J. J. Noël,[*] and D. W. Shoesmith[*]

Department of Chemistry, The University of Western Ontario, London, Ontario N6A-3K7, Canada

Alloy 22 electrodes crevice corroded under constant current conditions in 5 M NaCl at 120°C accumulated damage predominantly in the form of intergranular corrosion. Electron backscatter diffraction was used to determine the relationship between the location of damage and the crystallographic features of the grains and grain boundaries. The alloy possessed an exceptionally high number of "special" (Σ3) grain boundaries, and an intergranular attack was observed on random grain boundaries not exhibiting this special grain boundary character. The high percentage of special boundaries offers one reason for the excellent crevice corrosion resistance of this alloy.
 [DOI: 10.1149/1.3272851]

Manuscript submitted October 23, 2009; revised manuscript received November 10, 2009. Published December 23, 2009.

Alloy 22 is a Ni–Cr–Mo–W alloy (weight percent composition: 56Ni, 22Cr, 13Mo, 3W) with excellent corrosion resistance in aggressive environments but can exhibit susceptibility to stress corrosion cracking and crevice corrosion[1-3] when polarized at high temperatures in saline solutions. In concentrated chloride solutions at 120°C, crevice propagation under constant current conditions preferentially proceeds by intergranular attack,[4] which is not unexpected because grain boundaries are known locations for defects. When present, secondary phases and intermetallic precipitates locate at these sites and commonly act as initiation sites for localized corrosion. An extensive review describes how secondary phases and boundary defects affect the intergranular corrosion (IGC) of various nickel-based alloys.[5] However, Ni–Cr–Mo alloys possess a homogeneous face-centered cubic lattice, free of secondary phases and precipitates,[6] although thermal aging (>700°C) can lead to grain boundary precipitates, enriched in Mo relative to the bulk matrix.[7-10] Because the temperatures required to induce secondary phase formation are well beyond the temperatures used in the studies described here (120°), aging is not an issue.

Finding contrast in alloying element concentrations along grain boundaries and adjacent grains in Ni–Cr–Mo alloys is extremely difficult even with the most sensitive surface techniques.[11] Therefore, the mechanism for crevice initiation and propagation via IGC on Ni–Cr–Mo alloys is still unclear. We have used electron backscatter diffraction (EBSD) to relate corroded sites to grain boundary properties on alloy 22 surfaces.

Experimental

Alloy 22 electrodes were cut from an as-received, mill-annealed bulk sheet from Haynes International with no additional applied heat-treatment. Because alloy 22 was resistant to crevice corrosion under open-circuit conditions, we galvanostatically forced initiation and propagation. The crevice and electrochemical cell arrangements have been described previously in Ref. 12. A homemade Ag/AgCl (saturated KCl) reference electrode was used to measure the potential of the working electrode. Only a single creviced area was used. This area was mechanically polished with a sequence of SiC papers (of grit sizes 320–1200), then more finely polished on microcloths with alpha alumina pastes in the particle size orders of 5, 1, 0.5, and 0.03 μm, and finished with a mixture of colloidal silica and alumina. The electrode was then rinsed and ultrasonically cleaned in a water/methanol mixture.

To enhance the EBSD pattern quality, specimens are usually electropolished to minimize surface roughness.[13] In our experiments, electropolishing was not performed to avoid any ambiguities in the nature and protectiveness of the passive film that could be introduced by an electropolishing procedure. Also, the aggressive acidic chemistry formed within the occluded region during galvanostatic propagation effectively mimicked an electropolishing process by eliminating polishing scratches in corroded areas.

Based on previous results,[12] currents of either 30 or 70 μA were applied to initiate and lightly propagate crevice corrosion, in a neutral 5 M NaCl solution at 120°C, to an accumulated charge of 1.3 C. This procedure produced flat, scratch-free, and lightly attacked grains and avoided any complications due to corrosion product accumulation.

EBSD analyses were performed at the Canadian Centre for Electron Microscopy at McMaster University, Hamilton, Ontario. An HKL channel 5 EBSD system with a JEOL 7000F scanning electron microscope (SEM) operated at 20 kV was used to obtain grain orientation data. A step size of 1 μm was used to map the data. The software program "VMAP" written by Humphreys[14] was used to analyze and map the EBSD data. The Brandon criterion[15] was used to classify the Σ boundaries. Confocal laser scanning microscope (CLSM) images were produced at The University of Virginia, Charlottesville, VA.

Results and Discussion

Figure 1 shows the electrode potentials measured during crevice corrosion. As previously observed,[12] the potential initially increases to maximum values of $E \sim 0.525$ and 0.3 V (vs saturated Ag/AgCl) for 70 and 30 μA, respectively. This potential is beyond the initiation threshold of 0.2 V, and subsequently the potential decreases to a steady-state value indicative of an active behavior.[12] For $t > 5000$ s, the potential at 70 μA increases steadily with superimposed events, suggesting that the crevice attempts repassivation.

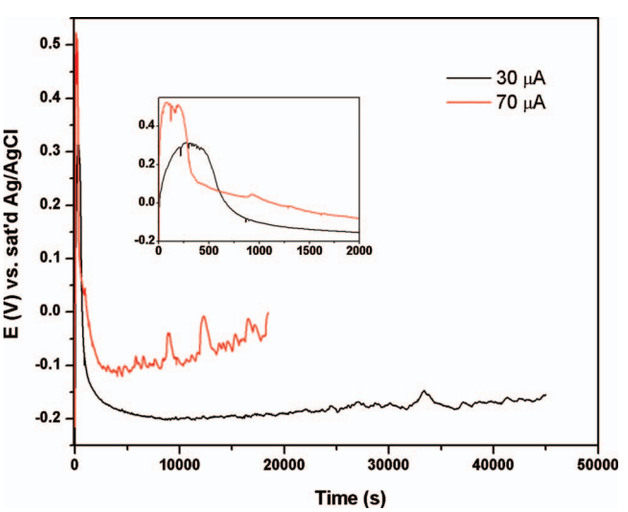

Figure 1. Measured potentials for applied currents of 30 (black) and 70 μA (red). The inset displays the initial rise in potential and its subsequent relaxation.

* Electrochemical Society Active Member.
[z] E-mail: pjakupi@uwo.ca

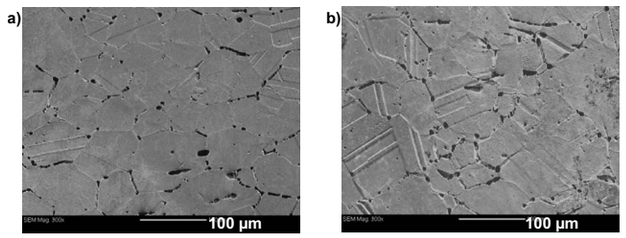

Figure 2. SEM micrographs of crevice-corroded regions for applied currents of (a) 30 and (b) 70 μA.

The SEM micrographs in Fig. 2 clearly show the grain boundaries within the corroded regions. For both specimens, some grain boundaries are decorated with pits and corroded intergranular channels. Damage to grain surfaces is either absent (30 μA) or minimal (70 μA). These results are confirmed by the CLSM image (Fig. 3), which shows that even at a substantially higher current of 200 μA, corrosion still travels across the creviced region, leaving behind pitted and channeled grain boundaries.[4] Figures 2 and 3 show that corrosion is generally confined to grain boundaries, but not all boundaries are attacked (compare A and B in Fig. 3). Because propagation occurs after the establishment of a critical chemistry characterized by low pH and high chloride content,[16,17] grains adjacent to corroded boundaries would experience similarly aggressive conditions, and a more uniform distribution of damage would be expected, especially for an alloy with a uniform microstructure. However, even locations only ~20 μm apart (A and B in Fig. 3) behave radically differently.

EBSD was used to detect whether differences in crystallographic orientations between the grains and the grain boundaries might be responsible for preferential initiation at intergranular sites. The atoms in the grain boundary region may be located at sites belonging to one, or the other, or both of the adjacent crystals if these were extended into the boundary space. These latter "coincident" sites would appear with a regular periodicity, and the ordered pattern is a coincidence site lattice (CSL). Misorientations between two grains can be related by an angle–axis pair that characterizes the CSL in a cubic system.[18] For example, a grain boundary with an angle–axis pair of $60°/\langle 111\rangle$ is characteristic of a $\Sigma 3$ boundary. The Σ notation denotes the reciprocal of coincidence points, and a $\Sigma 3$ boundary has one-third of its lattice points coincident to both adjacent grains. Grain boundaries with Σ values ≤ 29 ("special" boundaries) and low angle boundaries ($<15°$) possess extraordinary properties compared to high angle ($>15°$) "random" boundaries.[19,20]

Orientation maps are shown in Fig. 4, with the red lines delineating the $\Sigma 3$ grain boundaries, the yellow lines delineating the non-$\Sigma 3$ boundaries, and the black areas delineating the nonindexed corroded points. A statistical analysis shows that 57.7 and 50.2% of the grain boundary length segments are $\Sigma 3$ boundaries for the specimens corroded at 30 and 70 μA, respectively. These percentages are overestimates because the corroded nonindexed points are not

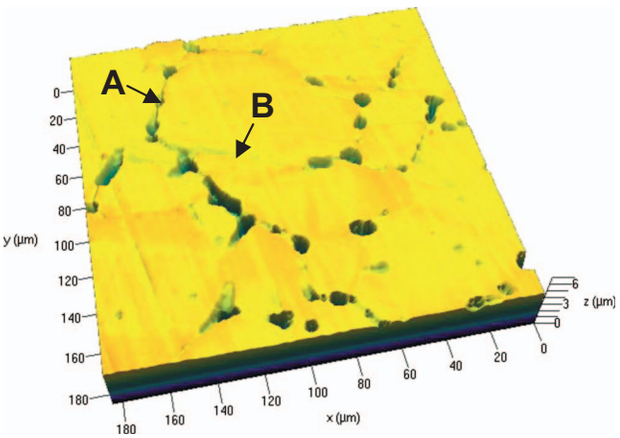

Figure 3. CLSM image within a corroded region of the creviced area on alloy 22 polarized at 200 μA.

counted, and the $\Sigma 3$ grain boundaries are usually longer compared to other special and high angle boundaries. Despite these uncertainties, these are high percentages considering that grain boundary engineering (GBE),[21] used to tailor the grain boundary distribution character, was not involved, and no special heat-treatment of the as-received alloy was undertaken. Typically, GBE processing increases the $\Sigma 3$ grain boundary content to $>50\%$, as shown for the Ni–Cr–Fe alloys, 600 [22] and 690.[23] Also, an increase in IGC resistance due to GBE processing of nickel,[22] aluminum,[24] and copper[25] has been attributed to the low Σ valued grain boundaries.

A total of 256 and 225 grain boundaries were analyzed for the 30 and 70 μA specimens, respectively; each grain and interconnecting boundary was analyzed individually; the analysis was simplified by grouping into $\Sigma 3$ and other non-$\Sigma 3$ boundaries. Figure 5 shows the total and relative percentages of uncorroded and corroded $\Sigma 3$ and other grain boundaries. Corrosion occurred exclusively on the non-$\Sigma 3$ boundaries at 30 μA and almost so at 70 μA. More than 90% of the non-$\Sigma 3$ boundaries were random and exhibit no special properties according to the CSL model.

Figure 6 shows an SEM magnification of the specimen corroded at 30 μA (i.e., of the surface shown in Fig. 2a) to emphasize the preferential corrosion at non-$\Sigma 3$ sites. Random and special boundaries are designated *R* and Σ, respectively. For clarity, the coherent $\Sigma 3$ twins were not outlined on all grains. For uncorroded boundaries not distinguished in the micrograph, a white line and a label are used to outline the special boundaries. Pitting commonly occurs at triple points, and IGC occurs along random boundaries. When corrosion is observed at a triple point involving a $\Sigma 3$ boundary, propagation occurs only along the random boundaries. In compiling Fig. 5, only the IGC along individual boundaries was counted, not that which occurred at locations shared by three joined boundaries. Boundary segments of $\Sigma 9$, 17, and 19 were also observed (Fig. 6), but due to

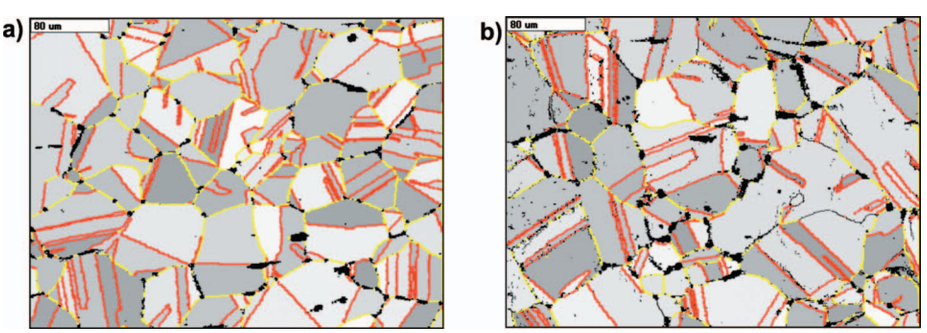

Figure 4. Orientation maps corresponding to micrographs from Fig. 2: (a) 30 and (b) 70 μA. Red and yellow delineate $\Sigma 3$ and non-$\Sigma 3$ boundaries, respectively. Black represents areas that could not be indexed due to corrosion and corrosion product accumulation.

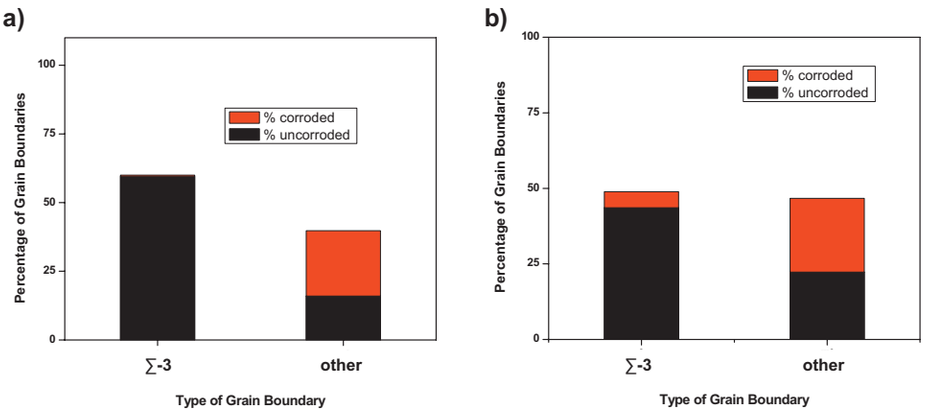

Figure 5. Percentage of uncorroded and corroded Σ3 and non-Σ3 grain boundaries for creviced alloy 22 specimens at (a) 30 and (b) 70 μA.

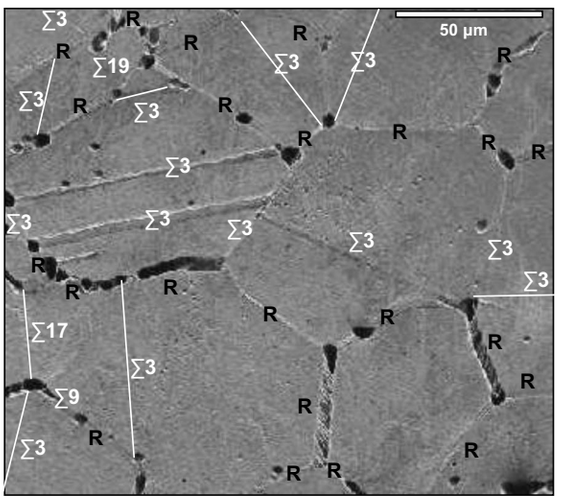

Figure 6. SEM of 30 μA corroded region emphasizing the trend of preferential attack along non-Σ3 boundaries, especially the random boundaries. White delineates Σ3 boundaries that appear as the bulk matrix in the micrograph, i.e., not corroded or etched. *R* represents random boundaries (Σ > 29).

the infrequency of non-Σ3 special boundaries, their corrosion resistance relative to the random boundaries cannot be assessed in this study.

Using EBSD studies with atomic force microscopy, Gray et al.[26] correlated crystallographic orientations and corrosion rates on planar disks (i.e., noncreviced specimens) of alloy 22. The corrosion resistance decreased in the grain orientation order {111} > {110} > {100}. We propose that the corrosion resistance of the {111} orientated grains was due, in large part, to the coherent Σ3 twin boundaries. Although the coherent twins are generally classified as Σ3 special boundaries, care should be taken when treating them synonymously because they have properties distinct from noncoherent Σ3 twins.[27,28]

To gain further insight into the superior corrosion resistance conferred by boundary orientations of alloy 22, one should link the boundary atomic chemistry with the alloying elements. Also, whether or not grain misorientations influence passive oxide film properties, the probability of initiation at these locations is not presently known.

Conclusions

Excellent EBSD pattern qualities of crevice-corroded regions on alloy 22 were obtained by electrochemically controlling the accumulated charge. Corrosion was observed to preferentially initiate at triple points (and non-Σ3 grain boundaries), and the subsequent attack propagated along random boundaries rather than along Σ3 boundaries. Because alloy 22 has an exceptionally high percentage of Σ3 boundaries, its crevice corrosion resistance can be attributed, at least partly, to grain orientation. It remains to be determined whether alloying elements play any role in determining grain boundary sensitivity to crevice corrosion.

Acknowledgments

The authors acknowledge Chris Butcher and Gianluigi Botton of the Canadian Centre of Electron Microscopy for their aid and use of the EBSD apparatus and John Humphreys (www.recrystallization-.info) for the use of VMAP software.

The University of Western Ontario assisted in meeting the publication costs of this article.

References

1. K. J. Evans, A. Yilmaz, S. D. Day, L. L. Wong, J. C. Estill, and R. B. Rebak, *JOM*, **57**, 56 (2005).
2. G. M. Gordon, *Corrosion (Houston)*, **58**, 811 (2002).
3. K. T. Chiang, D. S. Dunn, and G. A. Cragnolino, *Corrosion (Houston)*, **63**, 940 (2007).
4. P. Jakupi, J. J. Noël, and D.W. Shoesmith, To be published.
5. O. V. Kasparova, *Prot. Met.*, **36**, 524 (2000).
6. R. B. Rebak, in *ASM Handbook, Corrosion: Fundamentals, Testing, and Protection*, Vol. 13A, S. D. Cramer and B. S. Covino, Jr., Editors, p. 279, ASM International, Materials Park, OH (2003).
7. M. Raghavan, B. J. Berkowitz, and J. C. Scanlon, *Metall. Trans. A*, **13**, 979 (1982).
8. H. M. Tawancy, *J. Mater. Sci.*, **31**, 3929 (1996).
9. T. S. E. Summers, M. A. Wall, M. Kumar, S. J. Mathews, and R. B. Rebak, *Mater. Res. Soc. Symp. Proc.*, **556**, 919 (1999).
10. U. L. Heubner, E. Altpeter, M. B. Rockel, and E. Wallis, *Corrosion (Houston)*, **45**, 249 (1989).
11. Y.-M. Pan, D. S. Dunn, and G. A. Cragnolino, in *The Mike Meshii Symposium on Electron Microscopy: Its Role in Materials Research*, TMS (2003).
12. P. Jakupi, D. Zagidulin, J. J. Noël, and D. W. Shoesmith, *ECS Trans.*, **3**(31), 259 (2007).
13. G. L. Wynick and C. J. Boehlert, *Mater. Charact.*, **55**, 190 (2005).
14. http://www.recrystallization.info, last accessed Dec 8, 2009.
15. D. G. Brandon, *Acta Metall.*, **14**, 1479 (1966).
16. J. W. Oldfield and W. H. Sutton, *Br. Corros. J., London*, **13**, 13 (1978).
17. J. W. Oldfield and W. H. Sutton, *Br. Corros. J., London*, **13**, 104 (1978).
18. S. Ranganathan, *Acta Crystallogr.*, **21**, 197 (1966).
19. G. Palumbo and K. T. Aust, in *Materials Interfaces*, 1st ed., D. Wolf and S. Yip, Editors, p. 190, Chapman and Hall, London (1992).
20. T. Watanabe, *J. Phys. (Paris)*, **46**, C4 (1985).
21. P. Palumbo, Int. Pat. WO 94/14986 (1994).
22. P. Lin, G. Palumbo, U. Erb, and K. T. Aust, *Scr. Metall. Mater.*, **33**, 1387 (1995).
23. S. Xia, B. X. Zhou, W. J. Chen, and W. G. Wang, *Scr. Mater.*, **54**, 2019 (2006).
24. L. H. Chan, H. Weiland, S. Cheong, G. S. Rohrer, and A. D. Rollet, *Ceram. Trans.*, **201**, 261 (2009).
25. S. H. Kim, U. Erb, K. T. Aust, and G. Palumbo, *Scr. Mater.*, **44**, 835 (2001).
26. J. J. Gray, B. S. El Dasher, and C. A. Orme, *Surf. Sci.*, **600**, 2488 (2006).
27. V. Randle, *J. Mater. Sci.*, **40**, 853 (2005).
28. V. Randle, G. S. Rohrer, H. M. Miller, M. Coleman, and G. T. Owen, *Acta Mater.*, **56**, 2363 (2008).